

Pan-Antarctic assessment of ice shelf flexural responses to ocean waves

Jie Liang¹, Jordan P.A. Pitt¹, Luke G. Bennetts¹

¹School of Computer and Mathematical Sciences, University of Adelaide, Adelaide 5005, SA, Australia

Key Points:

- Crevasses and seabed protrusions create large ice shelf flexure in response to ocean waves
- Ice shelves that have experienced large scale calving events had much greater responses to swell than typical shelves
- Median ice shelf responses to swell are strongly correlated to median shelf front thicknesses

Abstract

Ice shelves flex in response to surface ocean waves, which imposes stresses and strains on the shelves that promote iceberg calving. Previous modelling studies of ice shelf responses to ocean waves have focussed on highly idealised geometries with uniform ice thickness and flat seabeds. This study leverages on a recently developed mathematical model that incorporates spatially varying geometries, combined with measured ice shelf thickness and seabed profiles, to conduct a statistical assessment of how fifteen Antarctic ice shelves respond to ocean waves over a broad range of relevant wave periods, from swell to infragravity waves to very long period waves. The results show the most extreme responses at a given wave period are generated by features in the ice shelves and/or seabed geometries, depending on the wave regime. Relationships are determined between the median ice shelf response and the median shelf front thickness or the median cavity depth. The findings provide further evidence of the role of ocean waves in large-scale calving events for certain ice shelves (particularly the Wilkins), indicate a possible role of ocean waves in calving events for other shelves (Larsen C and Conger), and the relationships determined provide a method to assess how ice shelf responses are evolving with climate change and project future scenarios.

Plain Language Summary

Antarctic ice shelves are the floating extensions of the Antarctic Ice Sheet that occupy over half of Antarctica’s coastline. They play a critical role in maintaining the stability of the Antarctic Ice Sheet by moderating the flow of grounded ice into the Southern Ocean. Climate change is causing them to thin and retreat, which is a major threat to global sea levels. Iceberg calving accounts for half of ice shelf loss, and ocean waves contribute to the calving process by rhythmically bending ice shelves. The influence of ocean waves on calving is expected to increase as the shelves and their surrounding sea ice barriers become weaker. Therefore, quantifying the responses of ice shelves to ocean waves is needed to project the future of the shelves. In this study, we use a recently developed mathematical model to conduct a statistical analysis of the responses of fifteen Antarctic ice shelves to ocean waves, ranging from storm waves to tsunamis. We show how features in the geometry can create large responses and we derive simple relationships between the responses and the geometry to aid projections of future scenarios.

1 Introduction

Antarctic ice shelves are weakening in response to climate change (Bennetts, Shakespeare, et al., 2023), thus reducing their buttressing effect on Antarctic Ice Sheet outflow (Gudmundsson, 2013), which is the primary cause of increasing mass loss (Noble et al., 2020; Fox-Kemper et al., 2021). Ice shelf weakening is equally caused by thinning and calving, both of which are likely to increase in rate in the future (Greene et al., 2022). Gradual weakening can cause ice shelves to become unstable and susceptible to large-scale calving events (referred to as disintegration, disaggregation or collapse) over short time periods (days to weeks), which can accelerate ice mass flow through the tributary glaciers (Rignot et al., 2004). These events are challenging to understand and model, which leads to deep uncertainties in projections of the Antarctic Ice Sheet’s contribution to future sea level rise (Oppenheimer et al., 2019).

Surface ocean waves cause ice shelves to flex, and the flexural stresses and strains imposed on the ice shelves were proposed as a mechanism for iceberg calving almost half a century ago (Holdsworth & Glynn, 1978). However, early field measurements of ice shelf flexure in response to ocean waves was limited to short signals (a few hours) on the Erebus ice tongue (e.g., Squire et al., 1994). A series of mathematical models of ice shelf flexure were developed, using a thin plate to model the ice shelf, coupled to a potential flow fluid to model the water motion in the sub-shelf cavity and open ocean (Holdsworth &

Glynn, 1978, 1981; Vinogradov & Holdsworth, 1985; Fox & Squire, 1991). Most models were two-dimensional (one horizontal dimension and one depth dimension), and assumed uniform ice thickness and a flat seabed. The model of Fox and Squire (1991), which predicts the response of an ice shelf to a regular incident wave from the open ocean, has been a benchmark for subsequent model developments.

Over the past one to two decades, two large-scale field measurement campaigns have been conducted on the Ross Ice Shelf (MacAyeal et al., 2006; Chen et al., 2019). They show the Ross Ice Shelf flexes in response to a broad range of ocean waves, from swell (wave periods 10–30 s; Cathles IV et al., 2009), to infragravity waves (50–300 s; Bromirski et al., 2010), to very long period waves (including tsunamis; 300–1000 s; Bromirski et al., 2017). There have also been observations linking calving of the Sulzberger Ice Shelf to the Honshu tsunami in 2011 (Brunt et al., 2011), and calving at the Larsen A and B and Wilkins Ice Shelf fronts caused by swell, which triggered runaway disintegration of the shelves (Massom et al., 2018). These findings have motivated further developments of mathematical models, which have gained the sophistication of spatially varying geometries (Ilyas et al., 2018; Papathanasiou et al., 2019; Meylan et al., 2021), combined extensional and flexural waves in the ice shelf (Kalyanaraman et al., 2020; Abrahams et al., 2023), and three dimensionality (Sergienko, 2017; Papathanasiou & Belibassakis, 2019; Tazhimbetov et al., 2023). Bennetts et al. (2022) integrated the Ross Ice Shelf thickness and seabed geometries from the BEDMAP2 dataset (Fretwell et al., 2013) into the model of Bennetts and Meylan (2021), and found model predictions for transfer functions (normalised ice shelf responses versus frequency) agreed well with the field measurements of Chen et al. (2019). Further, they used the model to show that, although the relative strain response of the Ross Ice Shelf to the incident wave amplitude is far greater for infragravity waves than for swell, the maximum strain responses to typical incoming swell and infragravity waves are similar, where the maximum responses to swell are localised (at crevasses), whereas the maximum responses to infragravity waves occur across the shelf.

In this study, we use the model of Bennetts and Meylan (2021) combined with the BEDMAP2 dataset (similar to Bennetts et al., 2022) to conduct the first pan-Antarctic study of ice shelf responses to ocean waves across a wave period range covering swell to infragravity waves to very long period waves. We include fifteen ice shelves in our statistical analysis, from all sectors of the Antarctic coastline and a range of ice shelf sizes. We study ice shelves that have experienced large-scale calving events (e.g., Larsen C and Amery) and disintegration/collapse (Wilkins and Conger) since their BEDMAP2 datasets were collected, along with the West Antarctic ice shelves currently experiencing rapid thinning and retreat (e.g., Thwaites and Pine Island). We find typical median responses for ice shelves, as identify ice shelves that have major differences from typical responses, particularly in the swell regime. We derive relationships between the median responses in the different wave period regimes and median properties of the geometry. Further, we show how geometrical features, such as crevasses and seabed protrusions, generate the most extreme ice shelf responses.

2 Mathematical model

Consider a transect stretching from the open ocean adjacent to an ice shelf front to the grounding zone of the ice shelf (Fig. 1). Let x denote the horizontal coordinate along the transect and z the vertical coordinate, where $x = 0$ is the shelf front and $z = 0$ is the free surface of the open ocean at rest. The transect occupies the interval $-l < x < L$, where l represents the extension into the open ocean from the shelf front and L is the ice shelf length. The geometry is defined by the location of the seabed, $z = -h(x)$ ($-l < x < L$), and the ice shelf draught and freeboard, respectively, $z = -d(x)$ and $z = f(x)$ ($0 < x < L$). Therefore, in the shelf-cavity interval ($0 < x < L$), the shelf thickness is $D(x) = f(x) + d(x)$ and cavity depth is $H(x) = h(x) - d(x)$.

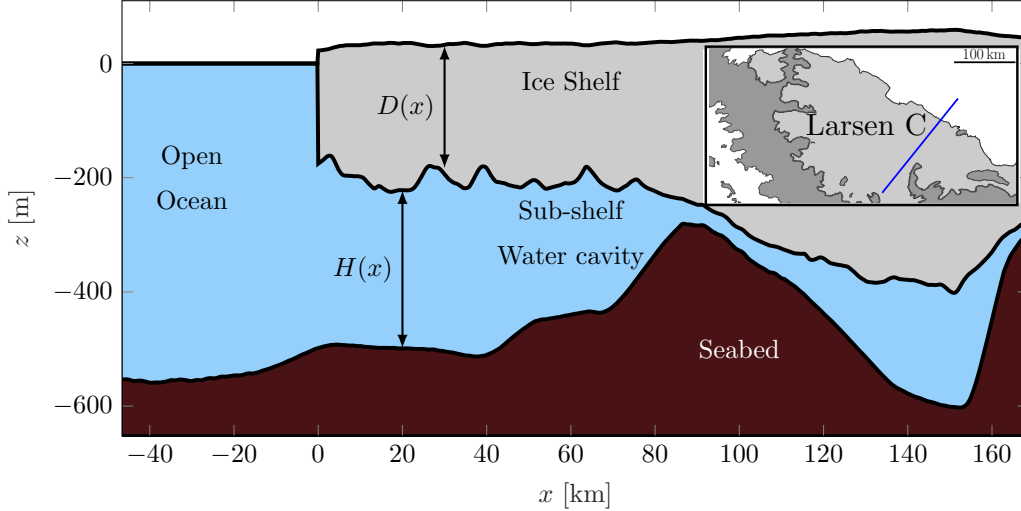


Figure 1. Schematic of the geometry (from BEDMAP2) along a transect through the Larsen C Ice Shelf (inset blue line).

Following standard water wave modelling practice, the water is assumed to be inviscid, incompressible and undergoing irrotational motion. Further, assuming small wave steepness (small amplitude relative to wavelength), linear and time-harmonic conditions are applied, such that the water velocity field at a prescribed angular frequency, ω , is defined as the gradient of

$$\text{Re} \left\{ (g A_{\text{inc}} / i \omega) \phi(x, z) e^{-i \omega t} \right\}, \quad (1)$$

where $g = 9.81 \text{ ms}^{-2}$ is the constant of gravitational acceleration, A_{inc} is an arbitrary incident amplitude, i is the imaginary unit, and $\phi \in \mathbb{C}$ defines the spatial dependence of the velocity potential at frequency ω . The (spatial component of the) velocity potential satisfies Laplace's equation,

$$\nabla^2 \phi = 0, \quad (2)$$

throughout the water domain, and Neumann boundary conditions (i.e., no normal flow) on the seabed and vertical face of the shelf front.

The ice shelf is modelled as a thin elastic (Kirchoff) plate with flexural rigidity $F(x)$. The underlying assumptions of the thin-plate model are that ice thickness is much less than the shelf length and the flexural wavelengths. Therefore, ice shelf flexure is defined by the vertical displacement of the water-ice interface, $\text{Re} \left\{ A_{\text{inc}} \eta(x) e^{-i \omega t} \right\}$, where $\eta \in \mathbb{C}$ in the displacement profile that contains information on magnitude (through its modulus) and phase (through its argument), which satisfies the plate equation

$$\{F \eta''\}'' + (\rho_w g - \rho_i \omega^2 D) \eta = \rho_w g \phi \quad \text{for } 0 < x < L, \quad (3)$$

where primes denote the derivatives with respect to x , and the right-hand side is forcing due to dynamic water pressure. The velocity potential and shelf displacement are also coupled through a standard kinematic condition (Bennetts et al., 2007), and free-edge conditions are applied at the shelf front ($x = 0$) (Bennetts, Williams, & Porter, 2023). In the open ocean ($-l < x < 0$), Eq. (3) collapses to the standard dynamic free-surface condition.

The flexural rigidity, F , is

$$F(x) = \frac{E D(x)^3}{12(1 - \nu^2)}, \quad (4)$$

Table 1. Ice shelf Young’s modulus values used in previous studies and their sources.

Article	E (GPa)	Source
D. G. Vaughan (1995)	0.88 ± 0.35	Field
Schmeltz et al. (2002)	0.8–3.5	Field
Lingle et al. (1981)	8.8	Field
Stephenson (1984)	9	Field
Robin (1958)	10	Field
Gammon et al. (1983)	9.3	Laboratory
Hutter (1983)	9.2–9.4	Laboratory
Petrovic (2003)	9.7–11.2	Laboratory
Fox and Squire (1991)	6	Unknown
MacAyeal and Sergienko (2013)	10	Unknown
Bromirski and Stephen (2012)	11	Unknown

where $\nu = 0.3$ is Poisson’s ratio and E is the (effective) Young’s modulus. A range of values have been used in the existing literature for the Young’s modulus of an ice shelf (Table 1). Field measurements tend to give smaller values than laboratory measurements, which is likely due to viscous deformation in the modelling of tidal flexure and data misinterpretation with grounded-ice dynamics (Sayag & Worster, 2013). Therefore, we discount these values, and set $E = 10$ GPa.

Motions are forced by an incident wave of amplitude A_{inc} from the open ocean. The incident wave excites flexural-gravity waves in the shelf–cavity region. Transmissive conditions are applied at the grounding line ($x = L$) to allow the flexural-gravity waves to propagate towards $x \rightarrow \infty$, i.e., out of the considered interval. Transmissive conditions are also applied at $x = -l$ to allow waves reflected by the shelf front back into the open ocean to propagate towards $x \rightarrow -\infty$.

The single-mode approximation (Bennetts et al., 2007; Bennetts & Meylan, 2021) is applied to the governing equations. Thus, the vertical structure of the velocity potential is restricted, such that

$$\phi(x, z) \approx \varphi(x) \cosh\{k(z + h)\} \quad \text{for} \quad -l < x < 0, \quad (5a)$$

$$\phi(x, z) \approx \psi(x) \cosh\{\kappa(z + h)\} \quad \text{for} \quad 0 < x < L, \quad (5b)$$

where $k(x)$ and $\kappa(x)$ are the wavenumbers in the open ocean and shelf–cavity regions, respectively, which are the positive, real solutions of the dispersion relations

$$g k \tanh(kh) = \omega^2 \quad \text{and} \quad \{F \kappa^4 + \rho_w g - \rho_i \omega^2 D\} \kappa \tanh(\kappa H) = \rho_w \omega^2. \quad (6)$$

In regions of uniform geometry, the single-mode approximation results in an ice shelf displacement of the form

$$\eta(x) = a^{(\pm)} e^{\pm i \kappa x} + \sum_{j=1,2} b_j^{(\pm)} e^{\pm i \mu_j x}. \quad (7)$$

The wavenumbers μ_j ($j = 1, 2$) are typically complex, such that $\mu_2 = -\overline{\mu_1}$ (where the overbar denotes the complex conjugate) and support damped propagating waves (Bennetts, 2007; Williams, 2006). The plus/minus superscripts denotes rightwards (+) and leftwards (−) propagation/decay. As part of the single-mode approximation, jump conditions, which represent weak forms of continuity of pressure and horizontal velocity, are introduced at $x = 0$, where the wavenumber changes from k to κ (Bennetts et al., 2007).

The dynamic flexural strains, ϵ , and stresses, σ , imposed on the ice shelf are

$$\epsilon(x, t) = \text{Re} \left\{ \frac{1}{2} D(x) \eta''(x) e^{-i\omega t} \right\} \quad (8a)$$

$$\text{and } \sigma(x, t) = \text{Re} \left\{ \frac{1}{2(1-\nu^2)} E D(x) \eta''(x) e^{-i\omega t} \right\}. \quad (8b)$$

Both quantities are proportional to the second derivative of the displacement, and, thus, its modulus, $|\eta''|$, is treated as the primary quantity of interest and referred to as the *ice shelf response (to unit incident amplitude waves)*.

The step approximation is used to compute φ , ψ and η (G. L. Vaughan et al., 2009; Squire et al., 2009). The horizontal intervals in the open ocean ($-l < x < 0$) and shelf-cavity region ($0 < x < L$) are divided into subintervals of length Δx , where the values of l and L are adjusted to be multiples of Δx . The geometry in each subinterval is set to be uniform, with values chosen at the subinterval midpoints to be consistent with the true geometry. Analytical expressions are available in each subinterval, where the unknowns are defined up to two (in the open ocean) or six (in the shelf-cavity region) amplitudes. The solutions in adjacent subintervals are connected via continuities (for the shelf displacements) and jump conditions (in the water). The amplitudes are calculated using a recursive algorithm (Bennetts & Squire, 2009; Rupprecht et al., 2017), which completes the solution. The subinterval length is reduced until a desired accuracy is achieved (e.g., 200 m for the Larsen C Ice Shelf studied in §3.1).

3 Case study: Larsen C Ice Shelf

3.1 Transects

Following the method of Bennetts et al. (2022) for the Ross Ice Shelf, a family of parallel transects are generated in directions normal to the a line of best fit approximating the Larsen C Ice Shelf front. Adjacent transects have a 2 km separation, and cover the maximum possible contiguous region of the Larsen C that avoids isolated islands, which results in 70 transects over a 140 km wide region. The transects have different lengths, such that they terminate at locations where the water cavity depth is less than 20 m. Each transect extends 50 km from the true shelf front into the open ocean (e.g., Fig. 1).

3.2 Effects of geometrical features

The transect shown in Fig. 1 is used to illustrate the impact of features in the geometry on the shelf response ($|\eta''|$) to incident wave forcing. The true geometry along the transect is (re-)shown (Fig. 2a), above three artificial variants that will isolate the effects of geometrical features for certain wave regimes. The true geometry is consecutively simplified by setting a uniform draught, $d = d(0)$, whilst varying the freeboard to keep the true ice thickness (Fig. 2b), a uniform freeboard to give a uniform ice thickness, $D = D(0)$ (Fig. 2c), and a uniform seabed, $h = h(0)$, (thus, a full uniform geometry; Fig. 2d). The three stages of simplification will determine the effects of variations in ice draught variations, ice thickness variations and seabed variations, respectively. Using the uniform thickness equal to the shelf front thickness gives a useful comparison with the varying thickness in the swell regime, as the shelf front thickness determines the proportion of the incident wave transmitted into the shelf (see §4). The other uniform geometrical values are sampled at $x = 0$ for consistency.

For incident waves in the swell regime (e.g., $T = 10$ s; Fig. 3a), the shelf thickness variations govern the shelf response, as the responses for the true and uniform draught geometries are almost indistinguishable. Variations in the cavity depth have a negligible effect on the shelf response (responses for the uniform thickness and full uniform geometries have only minor differences). The shelf response for the true geometry increases

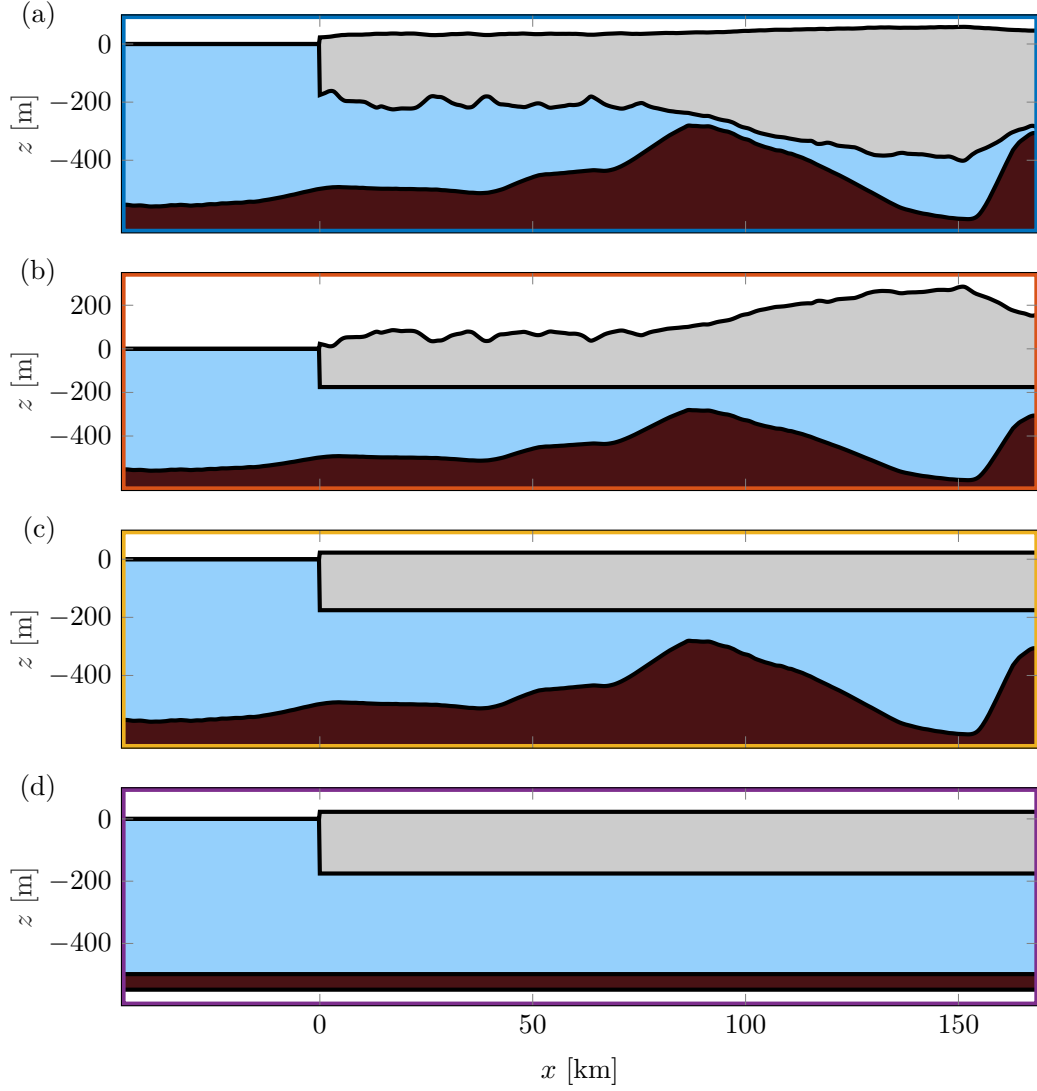


Figure 2. (a) True geometry, i.e., the transect through the Larsen C Ice Shelf, as in Fig. 1. (b–d) Consecutive simplifications of the true geometry along the transect: (b) uniform draught $d = d(0)$, with the freeboard varied to keep the true thickness; (c) uniform draught and freeboard, such that $D = D(0)$; (d) full uniform, with $d = d(0)$, $D = D(0)$ and $h = h(0)$. (The border colours correspond to the line colours in Fig. 3.)

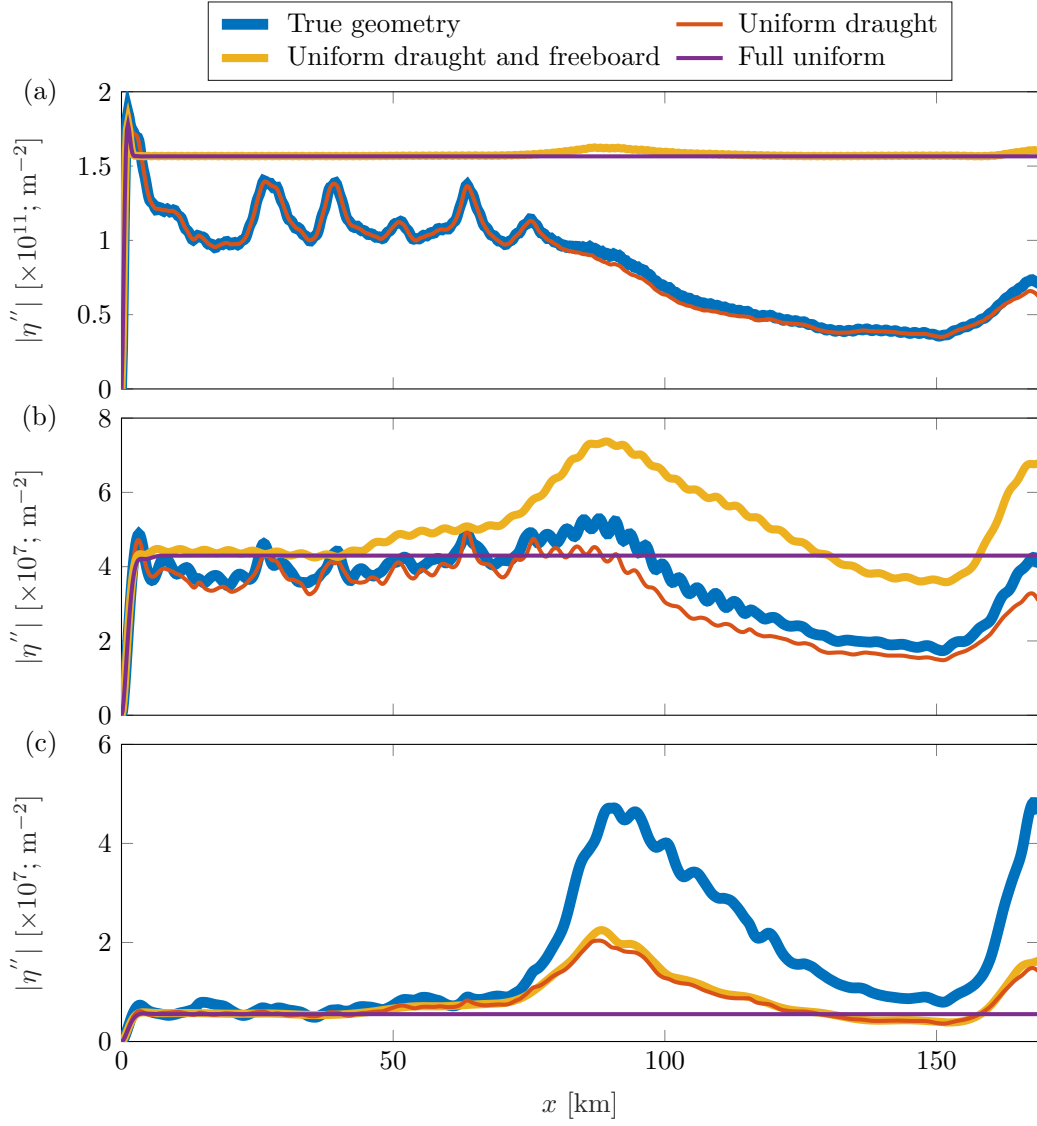


Figure 3. Ice shelf response profiles for the four geometries in Fig. 2 (line colours correspond to panel frame colours in Fig. 2), for wave periods (a) $T = 10$ s, (b) $T = 150$ s and (c) $T = 500$ s.

from zero at the shelf front (due to the free edge boundary conditions) to a peak over a short distance (order kilometres), which is the interval over which the damped propagating waves are active. Without thickness variations, the shelf response settles to an approximately constant value for the remainder of the shelf length. In contrast, with the thickness variations the response decreases as the ice thickens, particularly over approximately $0 < x < 75$ km, with local maxima appearing around thickness indentations.

For incident waves in the infragravity regime (e.g., $T = 150$ s; Fig. 3b), both the ice thickness and cavity depth variations influence the shelf response (all curves are distinct). The variations in the geometry are relatively small for approximately the first half of the interval ($0 < x < 75$ km), and the responses to all four geometries are similar over this interval. For $x > 75$ km, the ice thickens and there is a large protrusion in the seabed around $x = 90$ km, which cause the responses to separate. The responses for the true and uniform draught geometries remain similar, which indicates the ice thickness variations dominate the shelf response.

For incident waves in the very long period wave regime (e.g., $T = 500$ s; Fig. 3c), the cavity depth variations govern the shelf response, as responses for the uniform draught and uniform draught and thickness are almost indistinguishable. For the true geometry, the narrowing of the cavity around $x = 90$ km and towards the grounding zone cause large amplifications in the responses that reach over a factor of four greater than the mean value over $0 < x < 75$ km, where the response is relatively uniform. The amplifications drop to less than a factor of two for the uniform draught and uniform draught and thickness geometries, and are eliminated for the full uniform geometry. Therefore, variations in the cavity depth due to both the ice draught and seabed affect the response.

3.3 Analysis of multiple transects

The Larsen C responses to incident swell ($T = 10$ s) vary by orders of magnitude over the 70 transects (Fig. 4a). Most of the responses are clustered towards the smaller values, as indicated by the median response (blue curve). In contrast, the responses to infragravity waves ($T = 150$ s; Fig. 4b) and very long period waves ($T = 500$ s; Fig. 4c) are more closely packed around their median responses (blue curves), although the responses at given locations differ by more than twofold. The median responses are reasonably well approximated by responses for a full uniform geometry with thickness, draught and cavity depth values chosen as their respective medians over all transects (red curves). However, the responses for the median uniform shelf consistently underestimate the responses towards the shelf front, as the thickness of the median uniform shelf is typically greater than the true thickness towards the shelf front, and does not reproduce the gradual decrease in the response with distance along the shelf.

The overall median response of Larsen C (across all 70 transects) versus wave period (Fig. 5a) peaks in the infragravity regime ($T \approx 120$ s). It drops off slowly as wave period increases into the very long period regime, and rapidly as wave period decreases into the swell regime. As indicated by Fig. 4, the bulk of the responses at a given period (represented by the interquartile range; box) are spread over up to an order of magnitude for swell but tightly packed for infragravity and very long period waves (noting the logarithmic scale of the ordinate axis). However, the min-max range spreads over at least an order of magnitude for most of the wave period range, and is (relatively) greater in the very long period wave regime than the infragravity wave regime.

For incident swell ($T = 10$ s), the ten most extreme responses are clustered in two regions, with one region around the thinnest portion of the shelf front and the second region at the thinnest part of the grounding zone that corresponds to transects passing through thin sections of the shelf front (Fig. 5b). The most extreme responses for the very long period waves ($T = 500$ s) are also clustered in two patches, both where cavity depths become most shallow (Fig. 5c). The most extreme responses for the infragrav-

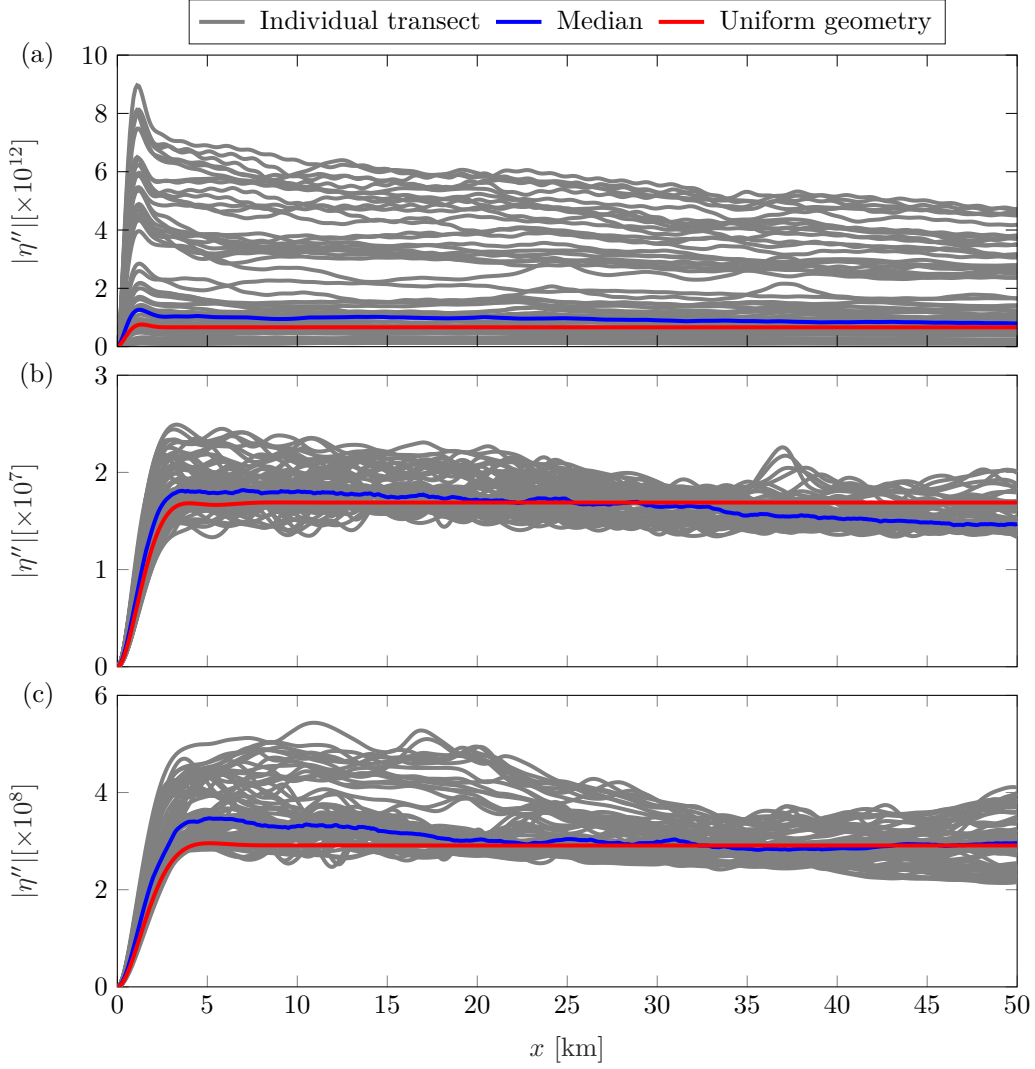


Figure 4. Shelf response profiles up to 50 km from the shelf front for 70 transects of the Larsen C Ice Shelf (grey curves), for wave periods (a) $T = 10$ s, (b) $T = 150$ s and (c) $T = 500$ s. The median responses at each spatial location (blue curves) and responses for the full uniform geometries using the median draught, thickness and cavity depth (red curves) are superimposed.

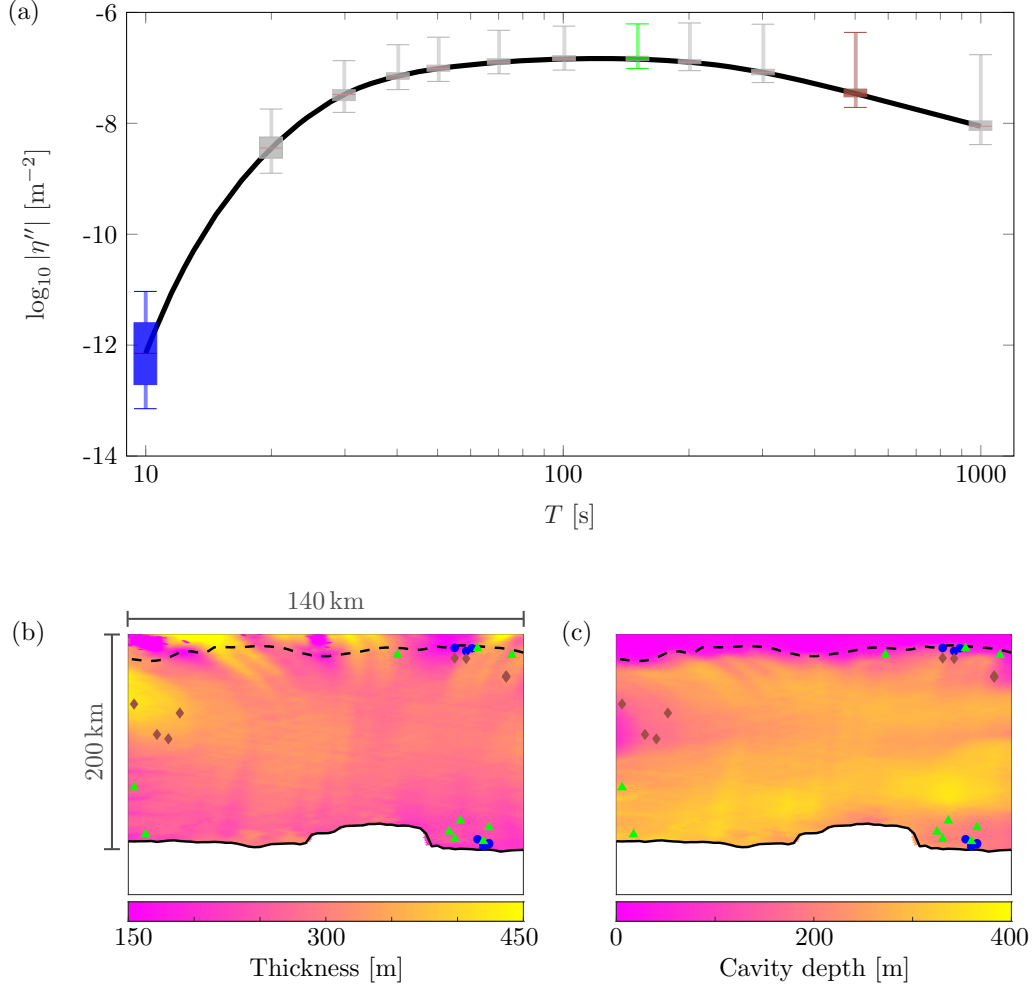


Figure 5. (a) Median response for Larsen C Ice Shelf versus wave period (for $x > 3$ km to avoid the shelf front boundary layer effect; black curve), with box and whisker plots at selected periods showing interquartile ranges and min-max responses, with $T = 10$ s (blue), $T = 150$ s (green) and $T = 500$ s (brown) highlighted. (b) Map of the Larsen C ice thickness over the region covered by transects, with the shelf front (black curve) and grounding line (broken curve) indicated, and locations of ten most extreme responses for $T = 10$ s (blue bullets), $T = 150$ s (green triangles) and $T = 500$ s (brown diamonds). (c) Similar to (b) but for the cavity depth map.

ity waves ($T = 150$ s) are more spread, and occur either where the shelf front is thin (Fig. 5b) or the cavity depth is shallow (Fig. 5c).

4 Statistical analysis of multiple ice shelves

The BEDMAP2 dataset (Fretwell et al., 2013) is used to study fifteen Antarctic ice shelves (Fig. 6a), covering all major sectors of the coastline and a range ice shelf sizes. For all of the ice shelves except the Wilkins and Conger (which have disintegrated/collapsed since the BEDMAP2 dataset was compiled), the median responses versus wave period (Fig. 6b) have similar properties to those of Larsen C (Fig. 5a). They have peaks of order 10^{-8} – 10^{-7} m^{-2} in the infragravity regime (> 100 s), slow drop offs to order $\approx 10^{-9}$ – 10^{-8} m^{-2} as period increases into the very long period wave regime and rapid drop offs by multiple orders of magnitude as period decreases into the swell regime. On the log-scale shown, differences are most pronounced in the swell regime. Pine Island has the weakest response to swell as it has a thick shelf front (median $D(0) > 400$ m), dropping to order $\approx 10^{-16}$ m^{-2} at $T = 10$ s, which is at least two orders of magnitude less than the other shelves. In contrast, the Voyeykov and Shackleton responses only drop to order 10^{-11} m^{-2} at $T = 10$ s, which is at least two orders of magnitude greater than most of the other shelves, as they have relatively thin shelf fronts (median $D(0) < 200$ m).

The Wilkins and Conger are the thinnest of the analysed ice shelves and their responses are different qualitatively and quantitatively from the other shelves. Their peak responses are $\approx 10^{-6}$ m^{-2} and occur at periods in the swell–infragravity wave transition (30–50 s). Their responses are orders of magnitude greater than those of the other shelves from the swell regime up to $T \approx 100$ s in the infragravity regime. They only drop to order 10^{-7} m^{-2} at $T = 10$ s, whereas they drop relatively rapidly as period increases into the very long period wave regime, such that their responses are less than many other shelves for $T > 600$ s.

In the swell regime, the median responses of the ice shelves decrease with increasing median shelf front thickness, $\langle D(0) \rangle$, such that the linear best fit

$$\log_{10} |\eta''| = -0.051 \langle D(0) \rangle - 14.827 \quad \text{for } T = 10 \text{ s}, \quad (9)$$

holds with a strong correlation (R -value of -0.991 ; Fig. 7a). The relationship is similar in the infragravity wave regime, although the median response is less sensitive to the shelf front thickness, e.g.,

$$\log_{10} |\eta''| = -0.06 \langle D(0) \rangle - 14.284 \quad \text{for } T = 150 \text{ s}, \quad (10)$$

and the correlation is weaker (R -value -0.884 ; Fig. 7b). In terms of the slope of the linear best fit, the sensitivity of the ice shelf response to the shelf front thickness decreases by an order of magnitude as wave period increases from $T = 10$ s to $T = 1000$ s (Fig. 9a). The intercept of the best fit differs only by factor ≈ 0.25 over the period range (Fig. 9b).

The relationship between the median shelf response and the median ice front thickness is lost in the very long period wave regime (e.g., R -value -0.316 for $T = 500$ s; Fig. 7c). In contrast, the median ice shelf response in the very long period wave regime is correlated with the median cavity depth, $\langle H \rangle$, such that the linear best fit

$$\log_{10} |\eta''| = -0.005 \langle H \rangle - 15.865 \quad \text{for } T = 500 \text{ s}, \quad (11)$$

holds with an R -value -0.945 (Fig. 8c). The responses at $T = 10$ s and 150 s are not correlated with the cavity depth (R -values -0.325 and -0.330 , respectively; Fig. 8a,b). There is a strong correlation ($|R\text{-value}| > 0.9$) between the median ice shelf response and the median shelf front thickness for $T \leq 200$ s (i.e., swell and most of the infragravity wave regimes) and the median cavity depth for $T \geq 400$ s (i.e., most of the very long period wave regime), with a crossovers in the correlations around $T = 300$ s (Fig. 9c).

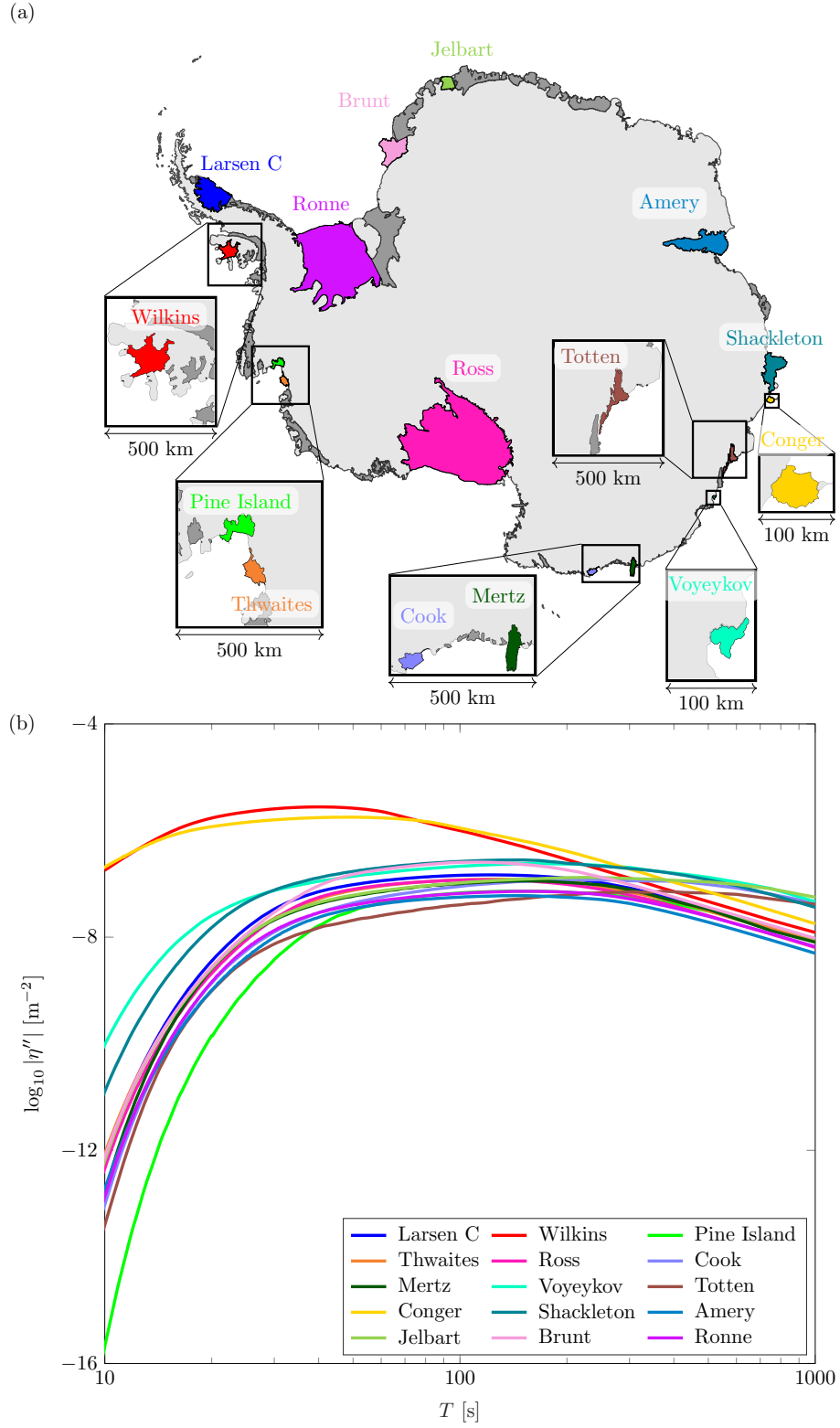


Figure 6. (a) Map of Antarctica, showing 15 ice shelves considered in the statistical analysis. (b) Log-log plot of the responses of each ice shelf versus wave period.

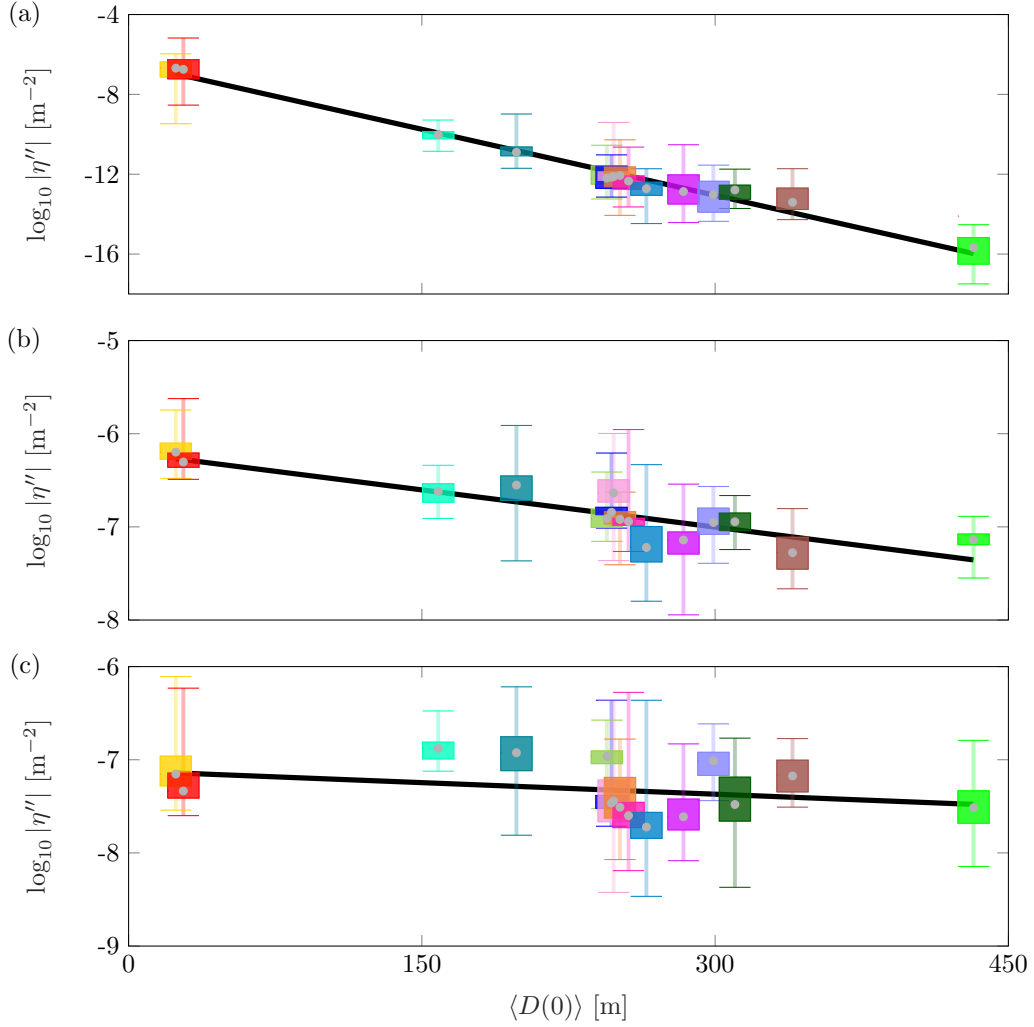


Figure 7. Responses of each of the 15 ice shelves versus median shelf front thickness, for (a) $T = 10$ s, (b) $T = 150$ s and (c) $T = 500$ s. The responses are represented as box and whisker plots (colours correspond to Fig. 6a), such that the boxes denote the interquartile ranges and whiskers are min-max values. Linear best fits (black lines) through the median responses (grey bullets) are shown.

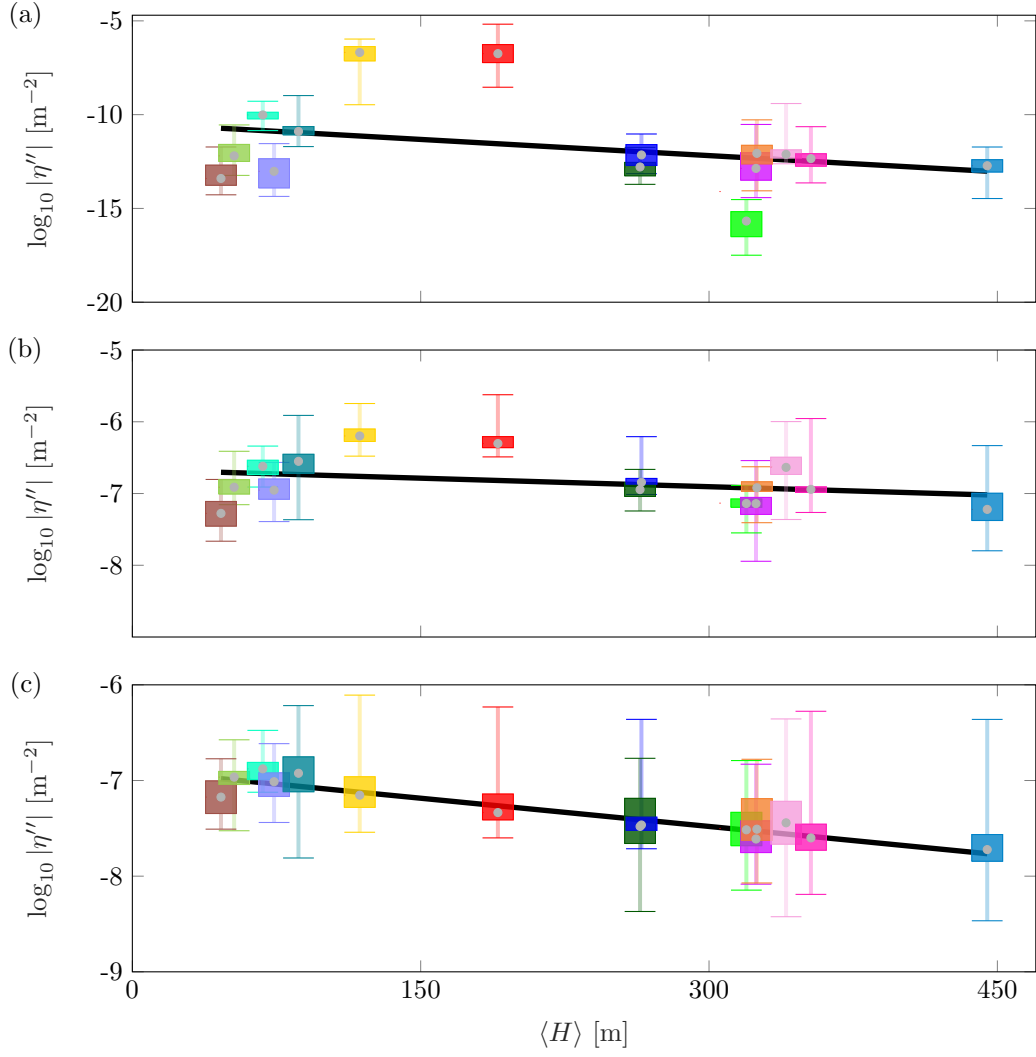


Figure 8. As in Fig. 7 but versus median cavity depth.

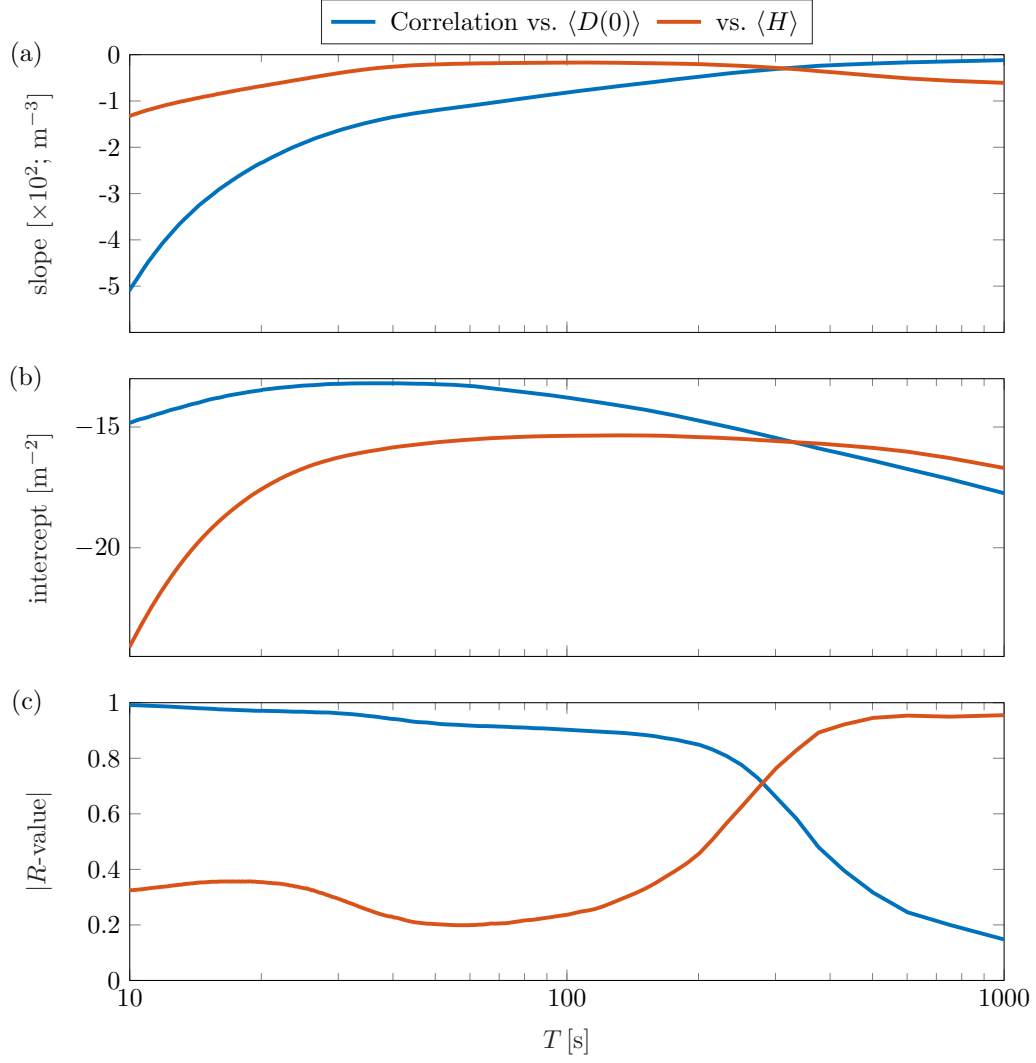


Figure 9. (a) Slope, (b) intercept and (c) modulus of R -values versus wave period, for linear relationships between \log_{10} of median ice shelf with shelf front thickness (red curve) and cavity depth (blue).

5 Conclusions and Discussion

A statistical analysis of the responses of fifteen Antarctic ice shelves to unit amplitude ocean waves, spanning swell to infragravity waves to very long period waves, has been conducted using a mathematical model that incorporates ice shelf geometries and bathymetries from the BEDMAP2 dataset (Bennetts & Meylan, 2021; Bennetts et al., 2022). Prior to the statistical analysis, a case study on the Larsen C Ice Shelf response revealed transitions in importance of geometrical features on the responses, as the incident wave period moved between the different regimes. Shelf thickness variations dominate responses to incident swell, whereas cavity depth variations dominate for very long period waves, with both shelf thickness and cavity depth variations influencing responses in the infragravity wave regime. Responses to swell were found to be most sensitive to the geometry, particularly the shelf front thickness, with the min-max range approximately two orders of magnitude over the Larsen C Ice Shelf for a 10 s wave period and the interquartile range an order of magnitude. The interquartile ranges for the responses in the infragravity and very long period wave regimes are relatively narrow (much less than an order of magnitude), although the min-max ranges are generally greater than an order of magnitude, mainly due to features in the geometry, such as protrusions in the seabed that reduce the cavity depth.

The median responses versus wave period were found to have similar characteristics for most of the ice shelves studied, with peaks of $\approx 10^{-7}$ – 10^{-6} m⁻² in the infragravity wave regime (≈ 150 s), slow drop offs as wave period increases into the very long period regime (generally less than an order of magnitude up to 1000 s), and rapid drop offs as wave period decreases into the swell regime (from two to eight orders of magnitude down to 10 s). In contrast, the two thinnest shelves studied (Wilkins and Conger) have far greater responses than the other ice shelves up to ≈ 150 s and particularly in the swell regime. The logarithm of the median responses of the ice shelves at a given wave period were shown to have a negative linear correlation with the median shelf front thickness in the swell regime and the infragravity wave regime up to ≈ 200 s, and with the median cavity depth in the very long period regime greater than ≈ 400 s.

The Wilkins and Conger Ice Shelves have similar responses to ocean waves, and both have experienced major calving events since their BEDMAP2 data were collected, leading to disintegration in 2008 and collapse in 2022, respectively. The relatively large responses of the Wilkins to swell (Fig. 6b and Fig. 7a), combined with the anomalously weak sea ice barriers in the lead ups to the calving events (Teder et al., 2022), is consistent with the hypothesis that swell triggered its calving events (Massom et al., 2018). Its response is relatively large for low period infragravity waves, so our findings are also consistent with infragravity waves triggering the calving events, as proposed by Bromirski et al. (2010). We are not aware of any implication in the literature to date that ocean waves played a role in the Conger Ice Shelf collapse. Our results suggest this possibility should be considered.

A giant tabular iceberg (A68) calved from the Larsen C Ice Shelf in 2017 (Larour et al., 2021), i.e., five years after the BEDMAP2 dataset was released. The predicted responses of the Larsen C do not indicate it as being any more susceptible to ocean waves than the other shelves (Figs. 6–8). The more recent BedMachine3 dataset has a higher spatial resolution than BEDMAP2 (450 m vs. 1 km; Morlighem et al., 2017). The updated geometry has almost no effect on the median response of the Larsen C (Fig. 10a). However, the distributions are far broader for the BedMachine3 dataset, by orders of magnitude and across the wave period spectrum (compare the boxes and whiskers in Figs. 5a and 10a). The most extreme responses to swell and infragravity waves for the BedMachine3 dataset are clustered around a crevasse network (Fig. 10b), which is not present in the BEDMAP2 dataset, and is close to the western end of the shelf front where the A68 iceberg calved. In contrast, the most extreme responses in the very long period regime

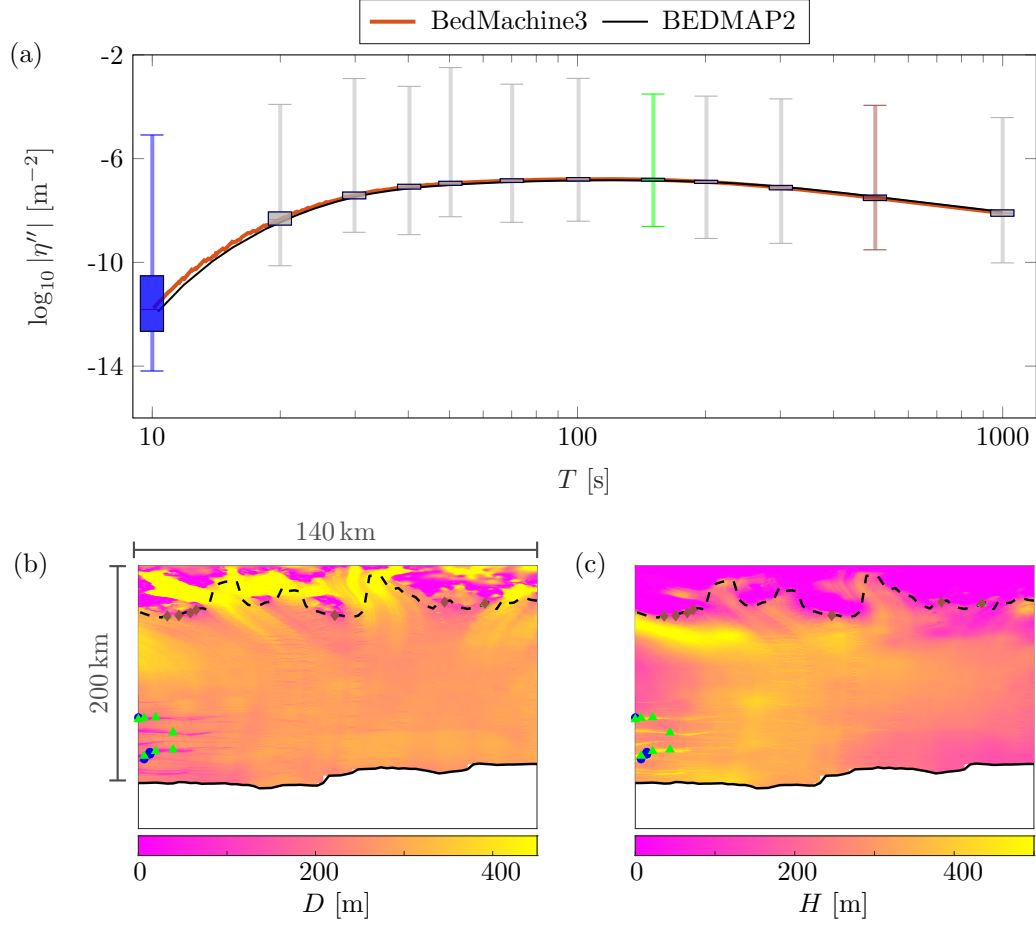


Figure 10. Similar to Fig. 5 but using geometries from the BedMachine3 dataset. The median response versus wave period using the BEDMAP2 dataset (see Fig. 5a) is superimposed on (a) for reference.

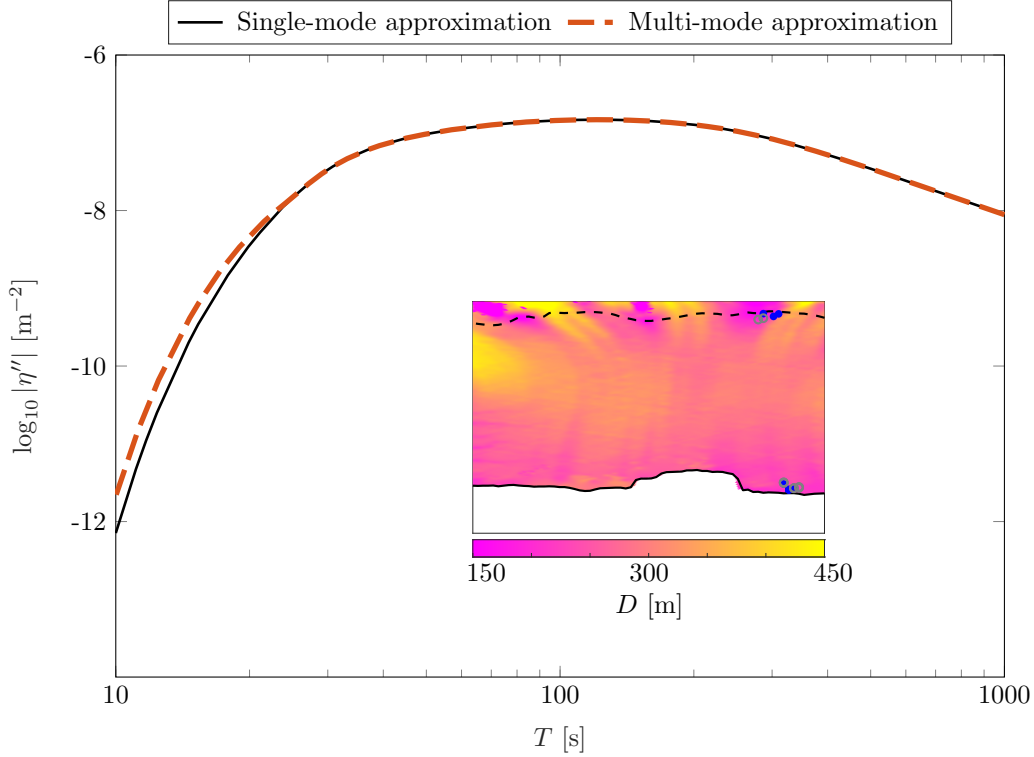


Figure A1. Larsen C Ice Shelf median response vs. wave period given by the single-mode approximation (black curve; as in Fig. 5a) and multi-mode approximation with ten evanescent modes (taken to be the full linear solution; red dashed). Inset shows ten most extreme responses at $T = 10$ s for the single-mode approximation (blue bullets) and multi-mode approximation (grey circles) superimposed on the Larsen C ice thickness map.

are clustered along the grounding line in a region where the cavity depth has a large gradient (Fig. 10c).

The linear relations we have derived between the median ice shelf responses and geometries give a benchmark to estimate the responses of other ice shelves and to predict how the responses evolve as the geometries respond to climate change. In particular, some Antarctic ice shelves have experienced major thinning since the BEDMAP2 dataset was compiled, such as the Thwaites and Pine Island. Therefore, it is likely that they will have much greater responses to swell than shown in our results, although this must be considered alongside any changes in the sea ice barriers. Moreover, our findings emphasise the need to incorporate geometrical features, such as crevasses from swell and cavity thinning for very long period waves, in order to model the most extreme responses of an ice shelf to waves and identify susceptible regions of the shelf.

Appendix A Multi-mode approximation

The multi-mode approximation extends the single-mode approximation by including a finite number of modes in ansatzes (5) that support evanescent (exponentially decaying) wave modes, i.e., with purely imaginary wavenumbers (Bennetts et al., 2007). The modes are ordered in increasing rate of decay. The multi-mode approximation is used to capture the full linear solution up to a desired accuracy by including a sufficient number of evanescent modes. The level of accuracy is typically judged by comparing approx-

iminations produced with differing numbers of modes. For the Larsen C, results are indistinguishable beyond ten evanescent modes (similar to Bennetts & Meylan, 2021), and the approximation with ten modes is taken to be the full linear solution. The median response for the full linear solution is indistinguishable from the single mode approximation beyond the swell regime ($T > 30$ s; Fig. A1). As expected, the single-mode becomes less accurate in as wave period decreases but the difference between the median responses in the swell regime is only a factor of three at worst. The distributions of responses for the full linear solution are also indistinguishable from the single-mode approximation for $T > 30$ s (not shown). In the swell regime, the most extreme responses are shifted slightly (Fig. A1 inset).

Open Research Section

The model outputs used for this study are available from the Australian Antarctic Data Centre (Liang et al., 2023).

Acknowledgments

JL is supported by a University of Adelaide PhD scholarship. The Australian Research Council and the Australian Antarctic Science Program funded this research (FT190100404, DP200102828, AAS4528).

References

- Abrahams, L., Mierzejewski, J., Dunham, E., & Bromirski, P. D. (2023). Ocean surface gravity wave excitation of flexural gravity and extensional Lamb waves in ice shelves. *Seismica*, 2(1).
- Bennetts, L. G. (2007). *Wave scattering by ice sheets of varying thickness* (Unpublished doctoral dissertation). University of Reading.
- Bennetts, L. G., Biggs, N. R. T., & Porter, D. (2007). A multi-mode approximation to wave scattering by ice sheets of varying thickness. *Journal of Fluid Mechanics*, 579, 413–443.
- Bennetts, L. G., Liang, J., & Pitt, J. (2022). Modeling ocean wave transfer to Ross Ice Shelf flexure. *Geophysical Research Letters*, 49(21), e2022GL100868.
- Bennetts, L. G., & Meylan, M. H. (2021). Complex resonant ice shelf vibrations. *SIAM Journal on Applied Mathematics*, 81(4), 1483–1502.
- Bennetts, L. G., Shakespeare, C. J., Vreugdenhil, C. A., Foppert, A., Gayen, B., Meyer, A., ... others (2023). Closing the loops on Southern Ocean dynamics: From the circumpolar current to ice shelves and from bottom mixing to surface waves. *Authorea Preprints*.
- Bennetts, L. G., & Squire, V. A. (2009). Wave scattering by multiple rows of circular ice floes. *Journal of Fluid Mechanics*, 639, 213–238.
- Bennetts, L. G., Williams, T. D., & Porter, R. (2023). A thin plate approximation for ocean wave interactions with an ice shelf. *arXiv preprint arXiv:2309.01330*.
- Bromirski, P. D., Chen, Z., Stephen, R. A., Gerstoft, P., Arcas, D., Diez, A., ... Nyblade, A. (2017). Tsunami and infragravity waves impacting Antarctic ice shelves. *Journal of Geophysical Research: Oceans*, 122(7), 5786–5801.
- Bromirski, P. D., Sergienko, O. V., & MacAyeal, D. R. (2010). Transoceanic infragravity waves impacting Antarctic ice shelves. *Geophysical Research Letters*, 37(2).
- Bromirski, P. D., & Stephen, R. A. (2012). Response of the Ross Ice Shelf, Antarctica, to ocean gravity-wave forcing. *Annals of Glaciology*, 53(60), 163–172.
- Brunt, K. M., Okal, E. A., & MacAyeal, D. R. (2011). Antarctic ice-shelf calving

- triggered by the Honshu (Japan) earthquake and tsunami, March 2011. *Journal of Glaciology*, 57(205), 785–788.
- Cathles IV, L., Okal, E. A., & MacAyeal, D. R. (2009). Seismic observations of sea swell on the floating Ross Ice Shelf, Antarctica. *Journal of Geophysical Research: Earth Surface*, 114(F2).
- Chen, Z., Bromirski, P., Gerstoft, P., Stephen, R., Lee, W. S., Yun, S., ... Nyblade, A. (2019). Ross Ice Shelf icequakes associated with ocean gravity wave activity. *Geophysical Research Letters*, 46(15), 8893–8902.
- Fox, C., & Squire, V. A. (1991). Coupling between the ocean and an ice shelf. *Annals of Glaciology*, 15, 101–108.
- Fox-Kemper, B., Hewitt, H., Xiao, C., Aðalgeirsdóttir, G., Drijfhout, S., Edwards, T., ... others (2021). *Ocean, cryosphere and sea level change. climate change 2021: The physical science basis. contribution of Working Group I to the Sixth Assessment Report of the Intergovernmental Panel on Climate Change*. Cambridge University Press.
- Fretwell, P., Pritchard, H. D., Vaughan, D. G., Bamber, J. L., Barrand, N. E., Bell, R., ... others (2013). BEDMAP2: improved ice bed, surface and thickness datasets for Antarctica. *The Cryosphere*, 7(1), 375–393.
- Gammon, P., Kieft, H., Clouter, M., & Denner, W. (1983). Elastic constants of artificial and natural ice samples by Brillouin spectroscopy. *Journal of Glaciology*, 29(103), 433–460.
- Greene, C. A., Gardner, A. S., Schlegel, N.-J., & Fraser, A. D. (2022). Antarctic calving loss rivals ice-shelf thinning. *Nature*, 609(7929), 948–953.
- Gudmundsson, G. (2013). Ice-shelf buttressing and the stability of marine ice sheets. *The Cryosphere*, 7(2), 647–655.
- Holdsworth, G., & Glynn, J. (1978). Iceberg calving from floating glaciers by a vibrating mechanism. *Nature*, 274(5670), 464–466.
- Holdsworth, G., & Glynn, J. (1981). A mechanism for the formation of large icebergs. *Journal of Geophysical Research: Oceans*, 86(C4), 3210–3222.
- Hutter, K. (1983). *Theoretical glaciology: material science of ice and the mechanics of glaciers and ice sheets*. Reidel/Terra Pub Co.,
- Ilyas, M., Meylan, M. H., Lamichhane, B., & Bennetts, L. G. (2018). Time-domain and modal response of ice shelves to wave forcing using the finite element method. *Journal of Fluids and Structures*, 80, 113–131.
- Kalyanaraman, B., Meylan, M. H., Bennetts, L. G., & Lamichhane, B. P. (2020). A coupled fluid-elasticity model for the wave forcing of an ice-shelf. *Journal of Fluids and Structures*, 97, 103074.
- Larour, E., Rignot, E., Poinelli, M., & Scheuchl, B. (2021). Physical processes controlling the rifting of Larsen C Ice Shelf, Antarctica, prior to the calving of iceberg A68. *Proceedings of the National Academy of Sciences*, 118(40), e2105080118.
- Liang, J., Bennetts, L. G., & Pitt, J. P. A. (2023). *Data for: Pan-antarctic assessment of ocean wave induced flexural stresses on ice shelves, Ver. 1* [dataset]. Australian Antarctic Data Centre. Retrieved from https://data.aad.gov.au/metadata/AAS_4528_Multi_Shelf doi: 10.26179/x5r2-vz21
- Lingle, C. S., Hughes, T. J., & Kollmeyer, R. C. (1981). Tidal flexure of Jakobshavns Glacier, West Greenland. *Journal of Geophysical Research: Solid Earth*, 86(B5), 3960–3968.
- MacAyeal, D. R., Okal, E. A., Aster, R. C., Bassis, J. N., Brunt, K. M., Cathles, L. M., ... others (2006). Transoceanic wave propagation links iceberg calving margins of Antarctica with storms in tropics and Northern Hemisphere. *Geophysical Research Letters*, 33(17).
- MacAyeal, D. R., & Sergienko, O. V. (2013). The flexural dynamics of melting ice shelves. *Annals of Glaciology*, 54(63), 1–10.
- Massom, R. A., Scambos, T. A., Bennetts, L. G., Reid, P., Squire, V. A., & Stam-

- merjohn, S. E. (2018). Antarctic ice shelf disintegration triggered by sea ice loss and ocean swell. *Nature*, *558*(7710), 383–389.
- Meylan, M. H., Ilyas, M., Lamichhane, B. P., & Bennetts, L. G. (2021). Swell-induced flexural vibrations of a thickening ice shelf over a shoaling seabed. *Proceedings of the Royal Society A*, *477*(2254), 20210173.
- Morlighem, M., Williams, C. N., Rignot, E., An, L., Arndt, J. E., Bamber, J. L., ... others (2017). BedMachine v3: Complete bed topography and ocean bathymetry mapping of Greenland from multibeam echo sounding combined with mass conservation. *Geophysical Research Letters*, *44*(21), 11–051.
- Noble, T., Rohling, E., Aitken, A., Bostock, H., Chase, Z., Gomez, N., ... others (2020). The sensitivity of the Antarctic Ice Sheet to a changing climate: past, present, and future. *Reviews of Geophysics*, *58*(4), e2019RG000663.
- Oppenheimer, M., Glavovic, B., Hinkel, J., Van de Wal, R., Magnan, A. K., Abd-Elgawad, A., ... others (2019). *Sea level rise and implications for low lying islands, coasts and communities. in: IPCC Special Report on the Ocean and Cryosphere in a Changing Climate.* The Intergovernmental Panel on Climate Change.
- Papathanasiou, T. K., & Belibassakis, K. A. (2019). A nonconforming hydroelastic triangle for ice shelf modal analysis. *Journal of Fluids and Structures*, *91*, 102741.
- Papathanasiou, T. K., Karperaki, A. E., & Belibassakis, K. A. (2019). On the resonant hydroelastic behaviour of ice shelves. *Ocean Modelling*, *133*, 11–26.
- Petrovic, J. (2003). Review mechanical properties of ice and snow. *Journal of Materials Science*, *38*, 1–6.
- Rignot, E., Casassa, G., Gogineni, P., Krabill, W., Rivera, A., & Thomas, R. (2004). Accelerated ice discharge from the Antarctic Peninsula following the collapse of Larsen B Ice Shelf. *Geophysical Research Letters*, *31*(18).
- Robin, G. d. Q. (1958). Norwegian-British-Swedish Antarctic Expedition, 1949–52. *Polar Record*, *6*(45), 608–616.
- Rupprecht, S., Bennetts, L. G., & Peter, M. A. (2017). Effective wave propagation along a rough thin-elastic beam. *Wave Motion*, *70*, 3–14.
- Sayag, R., & Worster, M. G. (2013). Elastic dynamics and tidal migration of grounding lines modify subglacial lubrication and melting. *Geophysical Research Letters*, *40*(22), 5877–5881.
- Schmeltz, M., Rignot, E., & MacAyeal, D. (2002). Tidal flexure along ice-sheet margins: comparison of insar with an elastic-plate model. *Annals of Glaciology*, *34*, 202–208.
- Sergienko, O. (2017). Behavior of flexural gravity waves on ice shelves: Application to the Ross Ice Shelf. *Journal of Geophysical Research: Oceans*, *122*(8), 6147–6164.
- Squire, V. A., Robinson, W. H., Meylan, M., & Haskell, T. G. (1994). Observations of flexural waves on the Erebus Ice Tongue, McMurdo Sound, Antarctica, and nearby sea ice. *Journal of Glaciology*, *40*(135), 377–385.
- Squire, V. A., Vaughan, G. L., & Bennetts, L. G. (2009). Ocean surface wave evolution in the Arctic Basin. *Geophysical Research Letters*, *36*(22).
- Stephenson, S. (1984). Glacier flexure and the position of grounding lines: measurements by tiltmeter on Rutford Ice Stream, Antarctica. *Annals of Glaciology*, *5*, 165–169.
- Tazhimbetov, N., Almquist, M., Werpers, J., & Dunham, E. M. (2023). Simulation of flexural-gravity wave propagation for elastic plates in shallow water using an energy-stable finite difference method with weakly enforced boundary and interface conditions. *Journal of Computational Physics*, *493*, 112470.
- Teder, N. J., Bennetts, L. G., Reid, P. A., & Massom, R. A. (2022). Sea ice-free corridors for large swell to reach Antarctic ice shelves. *Environmental Research Letters*, *17*(4), 045026.

- 497 Vaughan, D. G. (1995). Tidal flexure at ice shelf margins. *Journal of Geophysical*
 498 *Research: Solid Earth*, 100(B4), 6213–6224.
- 499 Vaughan, G. L., Bennetts, L. G., & Squire, V. A. (2009). The decay of flexural-
 500 gravity waves in long sea ice transects. *Proceedings of the Royal Society A*,
 501 465(2109), 2785–2812.
- 502 Vinogradov, O., & Holdsworth, G. (1985). Oscillation of a floating glacier tongue.
 503 *Cold Regions Science and Technology*, 10(3), 263–271.
- 504 Williams, T. D. C. (2006). *Reflections on ice: scattering of flexural gravity waves by*
 505 *irregularities in Arctic and Antarctic ice sheets* (Unpublished doctoral disserta-
 506 tion). University of Otago.